Precision and Accuracy in UHF-RFID Power Measurements for Passive Sensing

Cecilia Occhiuzzi and Gaetano Marrocco

***Abstract*— In spite of analog radio frequency identification (RFID) sensors are gaining increasing attention from academic and industrial domains, their true applicability in the real world is still in question, since it is not clear whether and in which conditions the variation of the measured signals related to the sensing activity may be distinguished from the measurement uncertainties. The RFID platform for analog sensing, namely, with no dedicated sensing electronics, is here characterized in term of precision and accuracy with reference to the arrangement and the reproducibility of the setup. Numerical analysis and laboratory experimentations demonstrated that the precision of power metrics measurement is twice the resolution of low-cost readers and that the uncertainty on the distance and the alignment may play a major role on the data accuracy. The environment-independent indicator, such as the analog identifier, revealed once again to be a very stable and robust metric. In overall, the obtained results suggest that analog RFID devices can be used as indicative sensing platform to identify a few levels of the phenomenon under observation. The sensing granularity can be improved using low-power ICs, while classification algorithms could be applied to increase the robustness of the detection.**

***Index Terms*— RFID sensor, measurement uncertainty.**

I. Introduction

THE application of radio frequency identification (RFID) technology for sensing procedures in addition to the more traditional logistic purposes is becoming a well established trend. In the last ten years several university laboratories have proposed devices that are able to label objects and at the same time to provide information about their state and modifications [1]. RFID sensing can be achieved by means of two different architectures. The *digital RFID sensing* makes use of RFID ICs with augmented sensing capabilities [2], [3], i.e. they include low power micro controllers, AC/DC converters and I/O ports for connecting general-purpose sensors. The *analog RFID sensing* relies instead on the straightforward evidence that the performance of an RFID tag is affected by the hosting object and hence it is possible to retrieve sensing data by just evaluating, at different times, the variation of the signals received and backscattered from the tags. Sensitive coating materials or lumped components displaced over the antenna, are also used to achieve a more specific response of the device [1].

Manuscript received July 2, 2015; revised January 20, 2016; accepted January 24, 2016. Date of publication February 8, 2016; date of current version March 16, 2016. The associate editor coordinating the review of this paper and approving it for publication was Dr. Lorenzo Lo Monte.

The authors are with RADIO6ENSE S.r.l. and the Pervasive Electromagnetics Laboratory, Univesity of Rome Tor Vergata, Rome 00133, Italy (e-mail: occhiuzzi@radio6ense.com; gaetano.marrocco@uniroma2.it).

Digital Object Identifier 10.1109/JSEN.2016.2526678

The first family of sensors are practically immune to the environmental interactions (data coming from the specific sensors are digitally encoded and transmitted through a regular RFID interrogation), and hence they can produce accurate and very selective outcomes. Devices of the latter family have instead generally lower cost but imply a critical trade-off between sensing and communication requirements. Accordingly, the dynamic range and the resolution of the measurement signals are limited by the minimum required interrogation distance and by the unavoidable uncertainties arising from the electromagnetic wave propagation into a practically random environment.

This paper will focus on this class of sensors since, although they are much less accurate than the digital RFID sensors, they are suitable to a potential mass diffusion within food and Pharma chains since they could be perceived as an augmented version of the well accepted tags for logistics.

A recent investigation on the fundamental bounds of analog RFID sensors [4] demonstrated how jointly mastering the sensing and the communication performance by solving a constrained impedance-matching problem. However, before RFID monitoring platforms may be effectively used in a real and unsupervised application, it is necessary to assess their true performance in term of precision and accuracy. In other words it is still an open question whether and in which condition it is possible to identify and discriminate the variation of the measured signals from the uncertainties of the measurement itself. This problem was partly investigated in [5] and [6] for what concerns methodologies and calibration procedures for the design and the characterization of RFID labels. In particular, it was demonstrated by means of ad-hoc test-beds, that backscattered power exhibits an overall uncertainty ranging from 0.5dB to 2dB with a strong sensitivity on the measurement instrumentation and onto the applied methodology. In a recent paper [7] the authors analyzed some sources of uncertainties, mostly related to misalignment, for particular measurement modes like the turn-on power and the analog identifier but only considering the identification of static tags. The performance of an RFID platform during a true sensor-oriented measurement session need instead to be systematized and experimented in a global vision including all the system variables.

The aim of this work is hence push the analysis of the RFID measurement accuracy forward a system level. Beside addressing the most important controllable parameters, we introduce other interrogation modes like the backscattered power at turn on, and we quantify the achievable resolution and accuracy in a realistic sensing-oriented measurement session, concerning

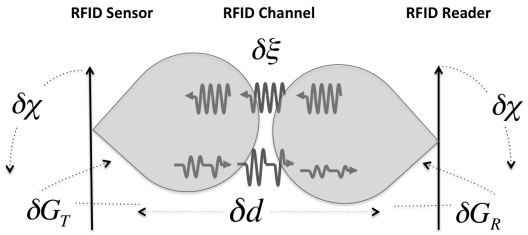

Fig. 1. Components (reader, propagation channel and tags) of an RFID platform for sensing purpose with indication of uncertainty sources $\{\delta G_R, \delta G_T, \delta\chi_P, \delta d, \delta\xi\}$ due to the misalignment (gain and polarization), distance, instrumentations and environment, respectively.

the monitoring of fluid level in a box, when the set-up is mounted and dismounted many times. The analysis will be mainly focused on static passive sensor network topologies, e.g. those setup wherein the mutual position between the reader and the tags can be considered stable or at least easily reproducible. The former category comprises long range fixed readers employed for monitoring a large number of RFID sensors dispersed in the environment. This may be the case of an industrial infrastructure where humidity, [8], deformation [9] and level sensors [10] are exploited for integrity and safety control, or of an agricultural warehouse in which it is necessary to constantly monitor the maturation levels of fruits and vegetables by using different chemical sensors [11]. In a reproducible scenario, instead, a fixed long range reader is used to monitor sensors displaced on objects undergoing a controlled movement, like goods on industrial conveyor belts. It is worth noticing that static networks represent a particular and simplified realization of RFID sensing platforms (mobile readers could be used as well [12]) and hence the outcomes of the this work should be considered as a baseline level for all the other network topologies.

The paper is organized as follow. After a theoretical formulation of the RFID Sensing Problem in Section II, the impact of the random or semi-random measurement conditions to the overall sensing precision is investigated in Section III. Section IV discusses the impact onto the measurement metrics of the non identical reproduction of the measurement setup with respect to a reference and calibrated one. Finally, a real case-study for the monitoring of the filling level of a box is presented in Section V to evaluate the true correlation between estimated and true data when all the error sources are present.

II. Formulation of the RFID Sensing Problem

An RFID sensing platform comprises the reader unit, the sensor tags and the communication channel (Fig.1) which hosts an asymmetric bi-directional link: the direct link from the reader to the tag and the reverse link from the tag to the reader. In the former case, the power emitted by the reader powers up the tag. In forward link, instead, the tag reflects back the wave coming from the reader and transmits its data by switching an internal impedance between two states at the aim of inducing a modulation of the carrier emitted by the reader. The communication produces two species of results that globally provide the *fingerprint* of the tag: a digital information, i.e. the digital identifier (ID) of the tag collected by the reader, and an analog information, i.e. a combination of the power levels corresponding to the two links. Any passive RFID tag may be theoretically transformed into a sensor through the integration with proper sensitive materials or even by just exploiting the variation of the antenna response to changing boundary conditions due to external agents [1]. Some readers are currently able to provide the phase of the backscattered field as well. However, since phase-oriented sensing procedures [13] are still in an embryonic age even for what concerns research, this paper will only focus on the effectiveness of the power-oriented sensing.

A. RFID Sensing Metrics

Let $\Psi(t)$ denote the local physical, chemical or geometrical parameter (temperature, humidity, gas concentration, deformation e.t.c.) of the environment surrounding the tag to be monitored by the RFID reader. Under simplified hypothesis, it is possible to derive two power metrics that are directly measurable by the reader: *i)* the turn-on power P_{in}^{to}, e.g. the minimum power requested to activate the tag for the specific arrangement of the setup, and *ii)* the backscattered power P_{bs}. Such metrics are related to the system parameters throughout the Friis and Radar equations:

$$P_{in}^{to}[\Psi] = \left(\frac{4\pi d}{\lambda_0}\right)^2 \frac{P_{chip}}{G_R(\theta,\phi)\chi_p G_T[\Psi](\theta,\phi)\tau\,[\Psi]} \quad (1)$$

$$P_{bs}[\Psi] = \left(\frac{\lambda_0}{4\pi d}\right)^4 P_{in} G_R^2(\theta,\phi) G_T^2[\Psi](\theta,\phi)\chi_p^2\rho[\Psi] \quad (2)$$

where d is the reader-tag distance, G_R is the gain of the reader antenna, $G_T[\Psi]$ is the gain of the tag's antenna at the specific realization of the process. P_{in} is the power feeding the reader's antenna. P_{chip} is the microchip sensitivity, e.g. the minimum RF power that the tag's antenna has to deliver to the microchip in order to activate it. χ_p is the polarization mismatch between the reader and the tag. $\tau[\Psi]$ is the power transmission coefficient of the tag

$$\tau[\Psi] = \frac{4R_{chip}R_a[\Psi]}{|Z_{chip} + Z_a[\Psi]|^2} \quad (3)$$

with $Z_a = R_a + jX_a$ antenna's input impedance and $Z_{chip} = R_{chip} + jX_{chip}$ the impedance of the microchip. $\rho = R_a/R_{chip}\tau$ is finally an impedance-dependent function. The backscattered power P_{bs} is measurable by the reader in terms of Received Signal Strength Indicator (RSSI) ([6], [14], [15]). Conversion formulas are reader-specific and are generally provided by the manufacturer.

By combining the forward (P_{in}^{to}) and backward (P_{bs}) powers, two new power metrics can be introduced. The *turn-on backscattered power* P_{bs}^{to} which is defined by introducing $P^{in} = P_{in}^{to}$ into (2) and the *Analog Identifier* (AID) [16]:

$$P_{bs}^{to}[\Psi] = \left(\frac{\lambda_0}{4\pi d}\right)^2 \frac{P_{chip}}{\tau\,[\Psi]} G_R(\theta,\phi) G_T[\Psi](\theta,\phi)\chi_p\rho[\Psi] \quad (4)$$

$$AID[\Psi] = P_{chip}/\sqrt{P_{bs}^{to}P_{in}^{to}} \quad (5)$$

AID is a non-dimensional indicator which was demonstrated to be theoretically independent on the reader-tag position and

on the interaction with the nearby environment, since it only depends on the antenna and microchip impedance as indicated in the following formula from [16]

$$AID[\Psi] = k_{AID}\frac{2R_{chip}}{\left|Z_{chip} + Z_a[\Psi]\right|} \tag{6}$$

where k_{AID} is a reader-specific constant that can be removed by calibration. AID is immune to the interrogation modalities and it is hence useful for non fixed measurements as when hand-held readers are used.

B. RFID Calibration Curves

Calibration curves are obtained experimentally or by the way of numerical simulations that relate values of the process under tests Ψ to the measured metrics $\xi = \{P_{in}^{to}, P_{bs}, P_{bs}^{to}, AID\}$. In particular, *data inversion curves* $\xi \leftrightarrow \Psi$ can be calculated at the purpose to guess the true value of $\Psi(t)$ from RFID measurements. It could be useful to normalize each indicator by its value in a particular reference state, say Ψ_0, for instance collected at the time of the tag placement into the environment to be monitored.

Calibration curves are obtained for a specific arrangement of the measurement system for what concerns the mutual reader/tag position and orientation as well as the emitted power and the nearby environment. Therefore the use of calibration curves in real conditions deserves some cares. In other words, apart from the case of AID, the inversion of power metrics implies an exact replication of the measurement reference conditions. Failure in this will produce errors and artifacts in the estimation of the real data. It is indeed necessary to investigate how an approximate control onto the measurement setup at different times, will affect the overall precision and accuracy of the RFID sensing system.

III. Precision of Power Data Measured by the Reader

Before getting into the problem of the accuracy of RFID sensing measurement it is appropriate to characterize the precision of RFID power data, as they are produced by the reader. The precision of the instrument, e.g. the agreement among different measured data, will be then compared in the next Section with the errors due to the specific measurement procedure.

The instrumental errors are intrinsic to the electronic components of the reader and are here grouped into two uncertainties over powers $\delta\xi = \{\delta P_{in}, \delta P_{bs}\}$. They superimpose on the measured turn-on power and on to backscattered power and propagate to the derived metrics AID and turn-on backscattered power. The $\xi \pm \delta\xi$ expressions will be considered later on for the evaluation of the system performance.

The precision of the reader for each metrics has to be evaluated through laboratory experimentations by performing repeated measurements at the same time and under the same conditions. At this purpose, the whole arrangement of the system (position and orientation of reader and tags) is assumed as fixed. The RFID interrogation takes less that 30ms and hence the channel can be accordingly considered as stationary during each measurement series.

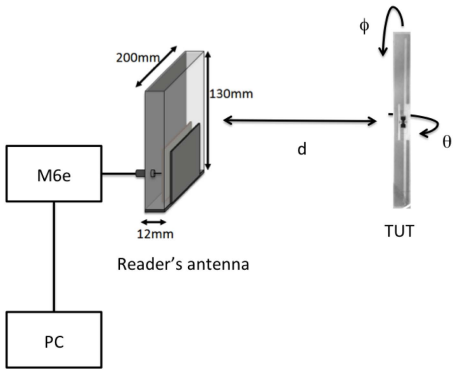

Fig. 2. Measurement setup for the characterization of the reader. The system comprises a dipole like-tag under test (TUT), the PIFA antenna and the M6e ThingMagic reader.

Let denote with $R(\xi)$ the resolution of the reader in the control of the feeding power and in the measurement of the backscattered power. On performing repeated measurements, the expected value is given by $\xi \sim \bar{\xi}_m \pm \sigma_\xi$ with σ the standard deviation and $\bar{\xi}_m$ the mean of all the different measured samples $\{\xi_{m1}, \xi_{m2}, ...\xi_{mn}\}$. If data acquisition produces equal or very similar samples as in the case of a low-resolution reader ($\xi_{m1} \simeq \xi_{m2} \simeq ....\xi_{mn}$) the resolution of the reader will mask the measurement errors ($R(\xi) \geq \sigma_\xi$). Accordingly, a single measurement can be enough to provide information about the true data as $\xi \sim \xi_m \pm R_\xi/2$.

The measurement of turn-on power and backscattered power do not have in general identical resolutions since they are correlated to different electronic subcomponents of the reader. Furthermore, the level of the turn-on power is significantly higher than the one of the backscattered power (30dBm vs. −50dBm). Accordingly, also their effects on the measured values in term of signal-to-noise ratio are expected to be different.

An example of characterization of the reader precision is now described with reference to the experimental setup in Fig. 2 which involves only off-the-shelf modules whose performance are fully representative of typical UHF RFID devices. The setup comprised a calibrated dipole-like tag (tag under test - TUT) and a typical long-range UHF fixed reader (ThingMagic M6e, [17]) suitable to be incorporated into a static RFID measurement setup. The manufacturer declares resolutions $R(P_{in}) = 0.5dB$ and $R(P_{bs}) = 1dB$. The reader was connected to a linearly polarized stacked PIFA antenna having beamwidths $BW_H = 85°$, $BW_V = 108°$, respectively on the horizontal (H) and vertical (V) planes.

The reader and the dipole tag were aligned in broadside direction ($\theta_0 = 0, \phi_0 = 0$) and were placed at four different mutual distances $d = \{40, 48, 50, 60\}cm$. Thirty six measurements were performed for each distance in the European UHF RFID band ($865.6 - 867.6MHz$), without modifying the standard frequency hopping procedures implemented by the reader. The turn-on method was applied for the measurements of P_{in}^{to} and P_{bs}^{to}, e.g. the power produced by the reader was gradually increased until the tag starts responding [18]. For the evaluation of P_{bs} the reader's power was instead kept fixed 5dB above the turn-on threshold to take into account

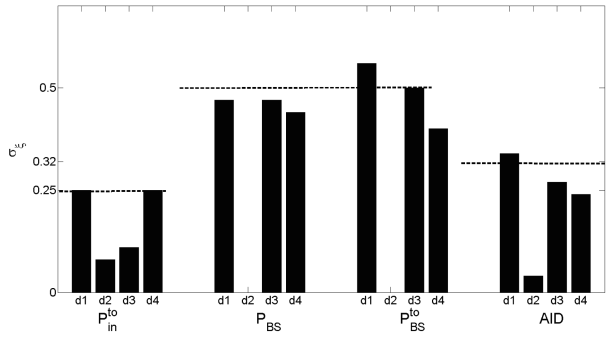

Fig. 3. Standard deviation σ_ξ for the four sensing metrics experimentally evaluated at different distances. Dashed lines indicates the corresponding half-resolutions $R(\xi)/2$ of the reader.

also the possible non-linearities induced to the IC due to the high impinging power. It is indeed known that when the power emitted by the readers is such that the power delivered to the IC exceeds 3 ± 5dB its threshold, the chip enters into a non linear behavior and its impedance deviates from the nominal one [19], [20].

Fig.3 shows the standard deviation σ_ξ for the four metrics, experimentally evaluated at the different distances, and compared with the half-resolution of the reader ($R(\xi)/2$). At the purpose of estimating also the precision of the AID data, the following propagation formula has been applied from (5) for the calculation of errors:

$$R(AID) = \left(R(P_{in}^{to}) + R(P_{bs}^{to})\right)/2 = 0.75dB \tag{7}$$

The standard deviation σ_ξ is always comparable with the half-resolution of the reader and in most cases it is even lower. The instrumental noise, the IC non linearities and the random fluctuations caused by the environment are hence masked by the resolution of the reader which therefore can be considered as fully representative of the precision of the measured data. For instance, the random uncertainties of the backward link in the dataset d2 (Fig. 3) are completely hidden by the reader resolution and accordingly the measurements are constant with zero standard deviation.

IV. Accuracy of Measurement Procedures for RFID Sensing

This section investigates the uncertainties that could overlay the estimation of RFID metrics when the measurement set-up deviates from the reference configuration used to produce the calibration curves. Such uncertainties are particularly relevant when an operator performs measurements at different times and has to mount and dismantle part of the equipment. The same considerations hold in case an hand-held device is used and, accordingly, the gain and distance can not be accurately controlled.

The geometry of the system arrangement is hereafter parametrized by variables $\mathbf{x} = \{d, \varphi, \theta\}$ describing the distance and the mutual orientation between the antennas of the reader and of the tag (as in Fig.1). $\mathbf{x}_0 = \{d_0, \varphi_0, \theta_0\}$ indicates the reference arrangement of the system and $\delta\mathbf{x} = \mathbf{x} - \mathbf{x}_0 = \{\delta d, \delta\theta, \delta\phi\}$ are the deviations from the reference setup geometry in successive independent measurements.

TABLE I
Sensitivity of Power Metrics to Channel Variability

	P_{in}^{to}	P_{BS}	P_{BS}^{to}
δd	2	4	2
δG_R	1	2	1
$\delta\chi_P$	1	2	1
δG_T	1	2	1

The incorrect replication of the orientation will impact on the gains of the antennas of the reader and of the tag, as well as onto the polarization matching even in case of curves normalized respect to a reference state Ψ_0. Such electromagnetic functions will hence experience a deviation $\{\delta G_R, \delta G_T, \delta\chi_P\}$ from their reference values. The non perfect replication of the distance, beside changing the interaction of radiated and backscattered field with the surrounding environment, could also introduce a perturbation of the input impedance of the chip due to the uncontrolled impinging power.

The weight of the various sources of uncertainty on the RFID metrics are evaluated by rewriting the expressions (1) and (2) in logarithmic form and making the dependance on such uncertainties as explicit:

$$\begin{aligned} P_{in}^{to} \approx\ & 2log\left(\frac{4\pi(d \pm \delta d)}{\lambda}\right) + (P_{chip} \pm \delta P_{chip}) \\ & - (G_R(\theta,\phi) \pm \delta G_R) - (G_T(\theta,\phi) \pm \delta G_T) \\ & - (\chi_P \pm \delta\chi_P) - \tau \pm \delta\tau \pm \delta P_{in} \end{aligned} \tag{8}$$

$$\begin{aligned} P_{bs} \approx\ & -4log\left(\frac{4\pi(d \pm \delta d)}{\lambda}\right) + (P_{in} \pm \delta P_{in}) \\ & + 2(G_R(\theta,\phi) \pm \delta G_R) + 2(G_T(\theta,\phi) \pm \delta G_T) \\ & + 2(\chi_P \pm \delta\chi_P) + (\rho \pm \delta\rho) \\ & \pm \delta P_{bs} \end{aligned} \tag{9}$$

$$\begin{aligned} P_{bs}^{to} \approx\ & -2log\left(\frac{4\pi(d \pm \delta d)}{\lambda}\right) \\ & + (G_R(\theta,\phi) \pm \delta G_R) + (G_T(\theta,\phi) \pm \delta G_T) \\ & + (P_{chip} \pm \delta P_{chip}) + (\chi_P \pm \delta\chi_P) + \rho \pm \delta\rho \\ & - \tau \pm \delta\tau \pm \delta P_{bs} \pm \delta P_{in} \end{aligned} \tag{10}$$

Above equations also include sources of uncertainty in the measurement due to the possible spread of the microchip sensitivity (δP_{chip}) among dies of a same manufacturer and can be removed by performing a self-calibration, like that of digital thermometers, at the time of the installation of the chip. The terms $\delta\tau$ and $\delta\rho$ are instead related to the above mentioned non linear behavior of the chip and impact only on P_{bs}, being all the other metrics evaluated at the turn-on condition [20]. Such uncertainties will not be theoretically analyzed anymore but will be nevertheless included into all the experimental test.

Tab.I summarizes the coefficients of the above sensing metrics, concerning the user-controllable parameters, which are useful to quantify the impact of each source of uncertainty. It follows that the backscattered power is expected to be more sensitive than the turn-on power to the random errors but it becomes much more robust when evaluated at the turn-on condition. Finally, the AID is affected only by the instrumental errors.

TABLE II
REPRODUCIBILITY INDIVIDUAL UNCERTAINTY $\varepsilon(\xi, x)$

	δd[cm]	$\delta\phi[°] \rightarrow \delta\chi$	$\delta\theta[°] \rightarrow \delta G$
P_{in}^{to}, P_{bs}^{to}	$0.08dB/cm$	$0.05dB/°$	$0.1dB/°$
P_{bs}	$0.17dB/cm$	$0.1dB/°$	$0.2dB/°$

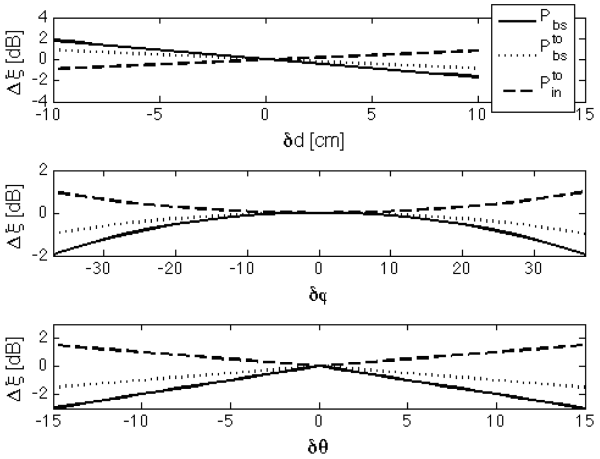

Fig. 4. Effects of the channel variability on the power metrics.

A. Numerical Analysis

Equations (8-10) are here numerically evaluated for the variations of distance $\delta d \in [-10, 10]cm$, orientation $\delta\varphi \in [-37, 37]°$, $\delta\theta \in [-15°, 15°]$ that correspond to a polarization mismatch $\delta\chi \in [-0.2, 0]$ between the reader and the tag and to a gain perturbation $\delta G \in [-1.5, 1.5]$dB. The reader antenna is assumed to have half-power beamwidth $BW = 60°$ [21]. The maximum changes of the three power metrics $\Delta\xi = \xi(x+\delta x) - \xi(x)$ are represented in Fig.4 while Table II shows their sensitivity to the geometrical parameters, $S_\xi = \partial\xi/\partial x$, as derived from Fig.4 through linearization.

The perturbation of the reader-tag distance and the misalignment are the dominant contributes, nevertheless the impact of small uncertainty on the geometry setup produces negligible effects onto the precision of the data. It is worth noting that a typical reader resolution of $R(P_{in}) = 0.5dB$ could mask a geometrical variation of the measurement setup up to $\delta x_{max} = \{6cm, 10°, 5°\}$.

However, the cumulative effect of the three sources of errors could be not negligible. A Monte Carlo analysis evaluated the behavior of the three metrics $\left\{P_{in}^{to}, P_{bs}, P_{bs}^{to}\right\}$ when subjected to a random variation of the channel parameters $\{d, \varphi, \theta\}$. Following the central limit theorem, a normal distribution over 2000 samples, comprised within the previous variation ranges was considered for each parameter. In the three cases (see the probability distribution in Fig. 5) the 60% of the samples of $\left\{P_{in}^{to}, P_{bs}, P_{bs}^{to}\right\}$ belongs to the $\pm$0.5dB interval ($\pm$1dB for P_{bs}) of the central value, corroborating the statements that the low reader resolution, in term of transmitted and received powers, could effectively mask the cumulative channel uncertainties. However, in the worst cases the uncertainties could reach up to 3dB for the turn-on metrics and 6dB in case of P_{bs} hence jeopardizing the entire sensing process.

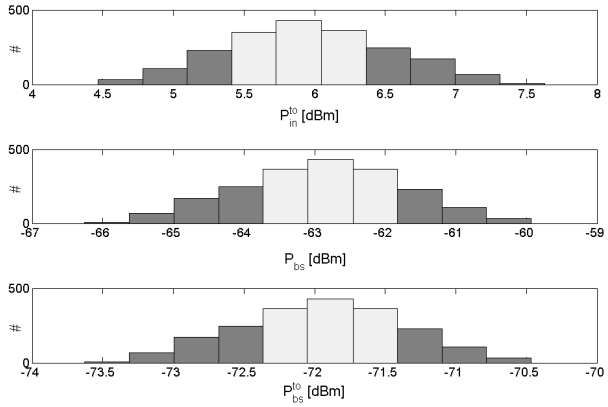

Fig. 5. Montecarlo analysis of the three metrics when the alignment parameters $\{d, \varphi, \theta\}$ are randomly changed according to a normal distribution. Lighter bars indicate the 60% of the samples occurring in the $\pm$0.5dB intervals ($\pm$1dB for P_{bs}) of the central value.

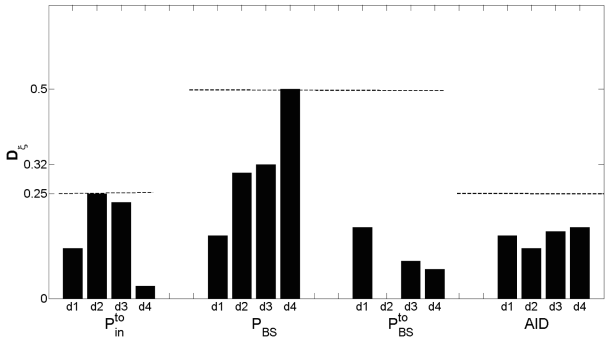

Fig. 6. Maximum half dispersion $D(\xi)$ for the four sensing metrics evaluated form measurement at different reader-tag distances $d = \{40, 48, 50, 60\}\,cm$. Dashed lines indicates the corresponding half-resolutions $R(\xi)/2$ of the reader.

It is worth noticing that all the previous analysis can be applied also to the uncertainties that affect the channel in term of scattering and reflection, by assuming that such phenomena produce distortions of the gain pattern and polarization.

B. Experimentation

The above numerical analysis is here corroborated by a laboratory experiment to evaluate the precision of RFID data against the manual replication of a same measurement conditions at different times. For each reader-tag distance $d = \{40, 48, 50, 60\}\,cm$ the setup of Fig.2 was dismantled and reproduced three times and the measured data were processed at the purpose to estimate the maximum half dispersions of the three sensing metrics $D(\xi) = (\xi_{MAX} - \xi_{min})/2$. Half maximum dispersion instead of standard deviation has been considered to process a small data set without committing statistical errors. Such indicator overestimates the errors and hence the analysis can be considered conservative.

Fig.6 shows $D(\xi)$ for the four distances together with the corresponding resolutions $R(\xi)/2$ of the reader. Also in this case, the perturbations on the measurement are masked by the reader resolution, as found in the numerical analysis, since almost in each case $D(\xi) \leq R(\xi)/2$. The first three power metrics $\{P_{in}^{to}, P_{bs}, P_{bs}^{in}\}$ look randomly affected by the reader-tag distance and the half-dispersion values are sensibly variable in the different measurement conditions, hence denoting

a not negligible effect of the environment, especially in the backscattered power P_{bs} while the P_{bs}^{to} is more stable due to the mitigation effect of the turn-on condition. The AID, which is environment-independent by construction, shows instead almost the same maximum dispersion, corroborating its robustness against channel variability.

The numerical and the experimental analysis suggest that the accuracy of RFID measurement in real conditions, provided that the reference measurement set-up is replicated with reasonable fidelity (a few centimeters and a few degrees), is fully comparable with the resolution low-cost readers.

V. A Real Case Study: Detection of the Filling Level

An example of calibration curve and of the characterization of the achievable resolution in realistic blind measurements is here given for what concerns the measurement of the filling level of a box [4]. The sensor was a T-match dipole [22] connected to the NXP-G2X microchip (input impedance $Z_{chip} = 16 - j148\Omega$ and power sensitivity $P_{chip} = -18dBmW$). The tag was used as sensor of the filling level of a perspex cylinder containing salty water (0.5g/l NaCl) by exploiting the perturbation of the antenna performance (gain and impedance) induced by the time-varying boundary conditions (the change of the local dielectric contrast of the box). The antenna was attached onto the external surface of the pipe (Fig.7) and it was designed (by using the electromagnetic numerical solver CST Microwave Studio 2014 [23]) to provide monotonic sensitivity ($S[\xi] = \Delta\xi/\Delta h$) of the turn-on power and of the AID to the filling level in the range of $0 < h < 3cm$ of the box, e.g. $S[P_{in}^{to}]$ =1.5 dB/cm and $S[AID] = 0.5dB/cm$, respectively. By considering the resolutions declared for typical commercial readers ($R(P_{in}) = 0.5dB$ and $R(P_{bs}) = 1dB$), the expected theoretical resolution [1] in the level measurement is hence 3mm for P_{in}^{to} and 15mm for AID.

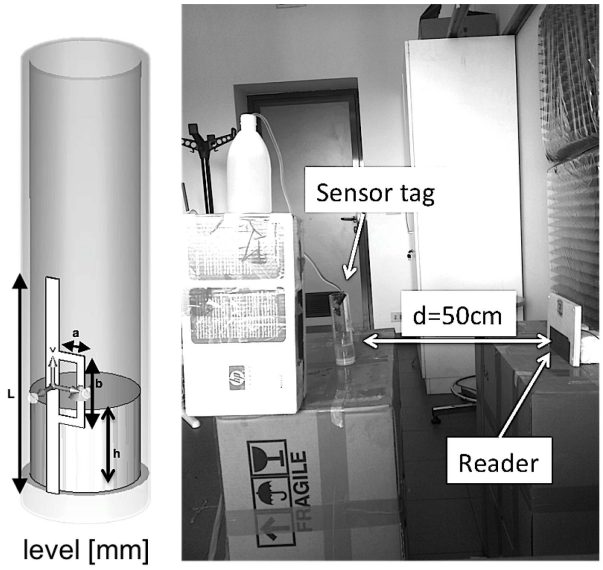

Fig. 7. Level sensor and measurement setup involving a T-match dipole with size L=78mm, a=10mm, b=20mm attached onto a plastic pipe filled with water of variable level h.

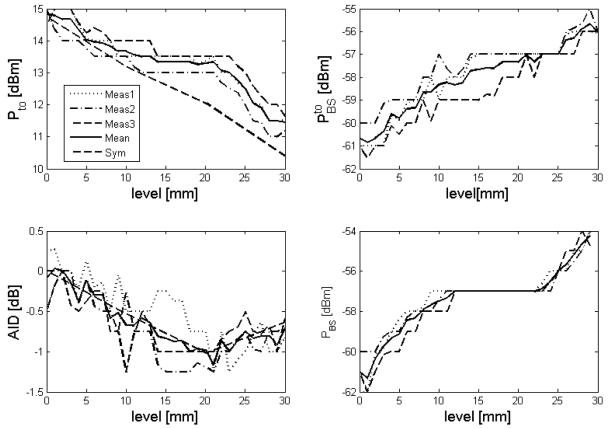

Fig. 8. Filling a container with a salty liquid. Measured and simulated RFID power metrics for the derivation of the calibration curves.

A. Calibration Curve

First, the above set-up was used to derive a calibration curve. The nominal geometrical parameter of the measurement arrangement were $\mathbf{x}_0 = d_0 = 50cm, \varphi_0 = \theta_0 = 0°$. The level of the liquid was gradually increased in a fully controllable way by exploiting the Torricelli's law. The turn-on power and the corresponding backscattered power at turn-on were measured as previously described. The backscattered power indicator was instead measured for fixed emitted power $P_{in} = 18dBm$.

Fig. 8 shows the measured results, their average and the comparison with the simulated profiles. Measurements and simulations are in good agreement in their absolute values and for what concerns the overall profiles. However, some discrepancies are visible in the central part of the diagrams where, unlike the expected results, the measured sensing curves P_{in}^{to} and P_{bs} exhibit indeed a flat profile. Furthermore, since the AID (which only depends on the antenna impedance) is instead well coherent with the simulation during the whole dynamics, the distortion of P_{in}^{to} and P_{bs} is likely related to the distortion of the gain of the two antennas probably due to the interaction with the environment that is not accounted by the simulations. Fig.9 gives the maximum dispersion $D(\xi)$ of the measurements compared with half the resolution of the reader for the considered metrics. It is apparent that the power measurements are less precise than in the static case of the previous Section (where there was no change in the tagged object) probably due to the combined and additive effect of all the uncertainty sources (distance, orientation, environment). The AID metric exhibits instead stable and lower dispersions during all the filling process.

In conclusion, the precision of the data in this set-up looks roughly twice the resolution of low-cost readers, e.g. it is precautionary to assume $\delta\xi \simeq R(\xi)$ for all the metrics except for the AID.

The calibration curves $h \leftrightarrow \xi \pm \delta\xi$ are finally derived from the previous experimental data by performing a polynomial (fourth-order) curve fitting (Fig.10). Although all the curves well fit to the experimental data ($R - square \geq 0.9$ over the same number of samples), their 95% confidence intervals

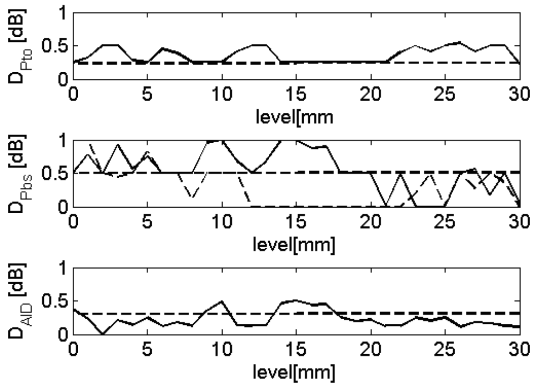

Fig. 9. Filling a container with a salty liquid. Maximum $D(\xi)$ compared with the corresponding resolutions of the reader $R(\xi)/2$.

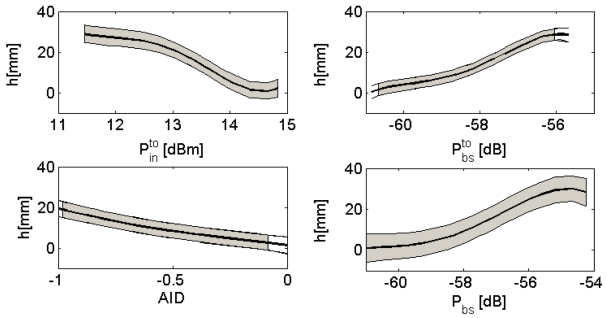

Fig. 10. Filling a container with a salty liquid. Calibration curves (thick lines), obtained from fourth-order polynomial curve fitting of Fig.8, together with indication of the 95% prediction intervals $h \pm \Delta h$.

appear sensibly different. As expected form theoretical and numerical analysis, AID and P_{bs}^{to} are the most precise indicators (average confidence interval of about 5-6 mm) while P_{bs} is the most variable parameter (average confidence interval of about 11mm). By considering $\delta\xi \simeq R(\xi)$ for all the metrics except for the AID ($\delta\xi = R(\xi)/2$), the maximum resolution in the detection of the filling lever is $R(h) = \{7, 8, 15, 8\}$mm for the turn-on power, turn-on backscattered power, AID and backscattered power, respectively which have to be compared with the values derived by the numerical analysis.

B. Accuracy of Data-Retrieval

All the errors and uncertainty sources were finally combined together within a blind experiment aimed at estimating the capability of the system to retrieve the filling level of the cylinder in a real environment by the only exploitation of the calibration curves.

The experiments were organized as follow: the cylinder was filled with the liquid up to a level $h_n = n\Delta h$, $\Delta h = 5mm$ and 20 measurement were performed. Data outliers were then removed before calculating the average values. Calibration curves in Fig.10 were used to guess the value of the level $\bar{\xi} \pm R(\xi) \rightarrow h \pm \Delta h$. Later on, the container was removed from the set-up, depleted, filled again up to another random level h_m, manually placed again in the measurement set-up approximately in the same position as before, and a new set of 20 measurements were taken. Since the repositioning was

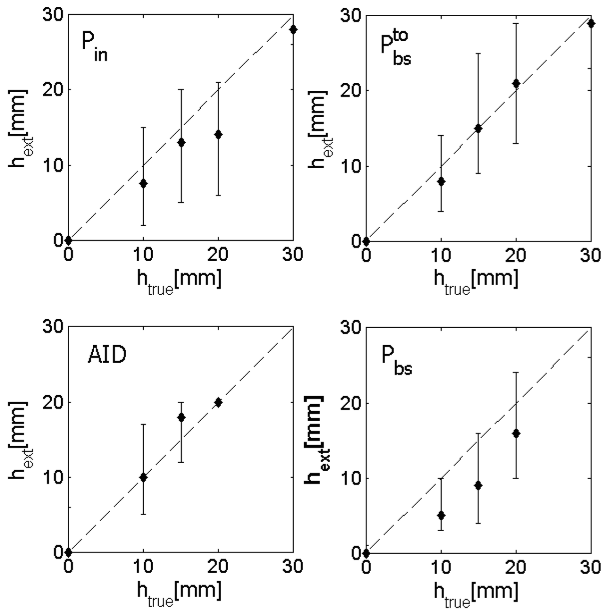

Fig. 11. Estimated filling level of the pipe vs. true ones by applying the fourth-order polynomial fitted calibration curves in Fig.10 when the power and AID sensing indicators are independently exploited.

done manually, the uncertainty on distance and on orientation of the tag was naturally introduced into the procedure.

Fig. 11 shows the comparison of the estimated levels of liquid with the real ones. The closer the values to the diagonal, the better is the overall system accuracy. As visible, most of the estimated data lie in close proximity of the diagonal, except for the two P_{in}^{to} and P_{bs} central values corresponding to the flat part of the calibration curves. Even in the worst case, at least one metrics properly intercepts the diagonal suggesting that a combined use of multiple parameters could sensibly improve the accuracy of the platform. Once again, P_{bs}^{to} and AID reveal the most accurate indicators.

Although the mean values of the four metrics look quite accurate, the uncertainties in the power data measurements ($\pm R(\xi)$) produce non negligible errors on the final data retrieval, with confidence intervals in the worst case of about $\Delta h \approx \{7, 8, 7, 6\}$ for the turn-on power, turn-on backscattered power, AID and backscattered power, respectively.

In principle, the overall variation of the liquid that the system is capable to sense could be enlarged by using a linear alignment of tags so that each of them is active in a sub-region of the water level. Although, the investigation of this specific problem is outside the scope of this work, it is expected that, once decomposed the dynamic range into sub-regions, the paper's outcomes can be directly applied to each sub-domain.

VI. Summary and Conclusion

The precision in the control of radiated power and in the measurement of backscattered powers is comparable with the resolution of low-cost readers. In a dynamic measurement, e.g. when the physical parameter under test is changing along with time, the precision of the power metrics could be however twice the reader resolution except for the AID whose dynamic precision looks similar as in the static case.

The uncertainty over the reader-tag distance and alignment plays a major role on the data accuracy but its effect looks negligible up to an uncertainty of about five centimeters or degrees. A reader-tag distance needs however to be known, at least roughly, during the measurement procedure. A sensing-oriented reader could be hence equipped with a distance/alignment measurement facility, for instance a low-cost laser meter. This information could be useful to correct the calibration curve or the specific set-up arrangement.

The AID indicator revealed once again a very stable and robust metric even if its dynamic range, and accordingly the corresponding sensing resolution, is generally lower that that of power metrics. Anyway, the considered metrics have some complementary features and may be jointly applied.

An overall and practical conclusion can be drawn by considering the upper bound in the balance between communication and sensing [1]. By assuming a dynamic range $\Delta\xi = 3dB$ of the sensing metric (e.g. by accepting a maximum degradation of the read distance less the 30% of the maximum one all along the time-varying physical phenomenon $\Psi(t)$), the number of grades of the phenomenon that a sensing RFID platform is really capable to discriminate, without additional processing, is at most just n=4 (in case of AID indicator). Hence the experienced limitations in term of uncertainties and achievable resolutions currently suggest a possible use of low-cost analog RFID sensors in *indicative sensing* systems aimed at providing, for instance, a few-levels scale of the freshness/quality of a good or of the environment. The Analog RFID sensing can be hence addressed as a classification problem and accordingly well assessed classification algorithms, like the Principal Component Analysis (PCA) could be applied to multiple indicators to improve the resolution and/or the detection robustness. Finally, unlike mathematically found by the authors in [1], there is no expected benefit to the number of achievable detectable levels by the use of more expensive higher resolution readers since the bottleneck of the measured procedure is still in the interaction with the environment and in the stability of the measurement set-up. Instead, the continuous improvement in the IC sensitivities (roughly 3dB each 2 years) may sensibly widen the available dynamic range of the sensors and hence the number of discriminable levels.

Finally, although all the simulations and tests concerned a static channel, it is worth noticing that the authors demonstrated in [16] and [24] that the AID is an invariant metric with respect to non stationary environments, also including moving obstacles. Accordingly the environment variability is expected to add only higher-order uncertainty at least in case the AID metrics is used.

REFERENCES

[1] C. Occhiuzzi, S. Caizzone, and G. Marrocco, "Passive UHF RFID antennas for sensing applications: Principles, methods, and classifcations," *IEEE Antennas Propag. Mag.*, vol. 55, no. 6, pp. 14–34, Dec. 2013.

[2] *EM 4325*. [Online]. Available: http://www.emmicroelectronic.com/, Apr. 2015.

[3] *SL900A*. [Online]. Available: http://ams.com/eng/Products/UHF-RFID/UHF-Interface-and-Sensor-Tag/SL900A, May 2014.

[4] C. Occhiuzzi and G. Marrocco, "Constrained-design of passive UHF RFID sensor antennas," *IEEE Trans. Antennas Propag.*, vol. 61, no. 6, pp. 2972–2980, Jun. 2013.

[5] D. G. Kuester, D. R. Novotny, J. R. Guerrieri, A. Ibrahim, and Z. B. Popovic, "Simple test and modeling of RFID tag backscatter," *IEEE Trans. Microw. Theory Techn.*, vol. 60, no. 7, pp. 2248–2258, Jul. 2012.

[6] A. Pouzin, T.-P. Vuong, S. Tedjini, M. Pouyet, J. Perdereau, and L. Dreux, "Determination of measurement uncertainties applied to the RCS and the differential RCS of UHF passive RFID tags," in *Proc. IEEE Antennas Propag. Soc. Int. Symp. (APSURSI)*, Jun. 2009, pp. 1–4.

[7] C. Occhiuzzi and G. Marrocco, "Uncertainty and applicability of RFID power measurements for passive sensing," in *Proc. 44th Eur. Microw. Conf. (EuMC)*, Oct. 2014, pp. 255–258.

[8] S. Manzari, C. Occhiuzzi, S. Nawale, A. Catini, C. Di Natale, and G. Marrocco, "Humidity sensing by polymer-loaded UHF RFID antennas," *IEEE Sensors J.*, vol. 12, no. 9, pp. 2851–2858, Sep. 2012.

[9] C. Occhiuzzi, C. Paggi, and G. Marrocco, "Passive RFID strain-sensor based on meander-line antennas," *IEEE Trans. Antennas Propag.*, vol. 59, no. 12, pp. 4836–4840, Dec. 2011.

[10] R. Bhattacharyya, C. Floerkemeier, and S. Sarma, "RFID tag antenna based sensing: Does your beverage glass need a refill?" in *Proc. IEEE Int. Conf. RFID*, Apr. 2010, pp. 126–133.

[11] S. Manzari, A. Catini, G. Pomarico, C. Di Natale, and G. Marrocco, "Development of an UHF RFID chemical sensor array for battery-less ambient sensing," *IEEE Sensors J.*, vol. 14, no. 10, pp. 3616–3623, Oct. 2014.

[12] *CAEN RFID*. (Jun. 2015). [Online]. Available: http://caenrfid.it

[13] M. C. Caccami, S. Manzari, and G. Marrocco, "Phase-oriented sensing by means of loaded UHF RFID tags," *IEEE Trans. Antennas Propag.*, vol. 63, no. 10, pp. 4512–4520, Oct. 2015.

[14] J. C. Bolomey, S. Capdevila, L. Jofre, and J. Romeu, "Electromagnetic modeling of RFID-modulated scattering mechanism. Application to tag performance evaluation," *Proc. IEEE*, vol. 98, no. 9, pp. 1555–1569, Sep. 2010.

[15] F. Fuschini, C. Piersanti, F. Paolazzi, and G. Falciasecca, "Analytical approach to the backscattering from UHF RFID transponder," *IEEE Antennas Wireless Propag. Lett.*, vol. 7, pp. 33–35, 2008.

[16] G. Marrocco, "RFID grids: Part I—Electromagnetic theory," *IEEE Trans. Antennas Propag.*, vol. 59, no. 3, pp. 1019–1026, Mar. 2011.

[17] *ThingMagic M6E*. [Online]. Available: http://www.thingmagic.com/index.php/fixed-rfid-readers/mercury6, accessed Jan. 2014.

[18] G. Marrocco and F. Amato, "Self-sensing passive RFID: From theory to tag design and experimentation," in *Proc. Eur. Microw. Conf. (EuMC)*, Oct. 2009, pp. 001–004.

[19] T. Bauernfeind, K. Preis, G. Koczka, S. Maier, and O. Biro, "Influence of the non-linear UHF-RFID IC impedance on the backscatter abilities of a T-match tag antenna design," *IEEE Trans. Magn.*, vol. 48, no. 2, pp. 755–758, Feb. 2012.

[20] P. V. Nikitin, K. V. S. Rao, R. D. Martinez, and S. F. Lam, "Sensitivity and impedance measurements of UHF RFID chips," *IEEE Trans. Microw. Theory Techn.*, vol. 57, no. 5, pp. 1297–1302, May 2009.

[21] G. Marrocco, E. Di Giampaolo, and R. Aliberti, "Estimation of UHF RFID reading regions in real environments," *IEEE Antennas Propag. Mag.*, vol. 51, no. 6, pp. 44–57, Dec. 2009.

[22] G. Marrocco, "The art of UHF RFID antenna design: Impedance-matching and size-reduction techniques," *IEEE Antennas Propag. Mag.*, vol. 50, no. 1, pp. 66–79, Feb. 2008.

[23] [Online]. Available: https://www.cst.com

[24] S. Caizzone and G. Marrocco, "RFID grids: Part II—Experimentations," *IEEE Trans. Antennas Propag.*, vol. 59, no. 8, pp. 2896–2904, Aug. 2011.

Cecilia Occhiuzzi, photograph and biography not available at the time of publication.

Gaetano Marrocco, photograph and biography not available at the time of publication.